Local Neutral Density and Plasma Parameter Measurements in a Hollow Cathode Plume

Kristina K. Jameson[*], Dan M. Goebel[†], Ioannis MiKellides[‡] and Ron M. Watkins[§],
Jet Propulsion Laboratory, California Institute of Technology, Pasadena, CA 91109

In order to understand the cathode and keeper wear observed during the Extended Life Test (ELT) of the DS1 flight spare NSTAR thruster and provide benchmarking data for a 2D cathode/cathode-plume model, a basic understanding of the plasma and neutral gas parameters in the cathode orifice and keeper region of the cathode plume must be obtained. The JPL cathode facility is instrumented with an array of Langmuir probe diagnostics along with an optical diagnostic to measure line intensity of xenon neutrals. In order to make direct comparisons with the present model, a flat plate anode arrangement was installed for these tests. Neutral density is deduced from the scanning probe data of the plasma parameters and the measured xenon line intensity in the optical regime. The Langmuir probes are scanned both axially, out to 7.0 cm downstream of the keeper, and radially to obtain 2D profile of the plasma parameters. The optical fiber is housed in a collimating stainless steel tube, and is scanned to view across the cathode plume along cuts in front of the keeper with a resolution of 1.5 mm. The radial intensities are unfolded using the Abel inversion technique that produces radial profiles of local neutral density. In this paper, detailed measurements of the plasma parameters and the local neutral densities will be presented in the cathode/keeper plume region for a 1.5 cm diameter NEXIS cathode at 25A of discharge current at several different strengths of applied magnetic field.

Nomenclature

A	=	probe area	n	=	plasma density
e	=	electron charge	M	=	ion mass
I	=	probe current	T_e	=	electron temperature
k	=	Boltzman's constant	β	=	Plasma ion current coefficient

I.   Introduction

Hollow cathodes are one of the most, if not the most, critical components of modern electric thrusters, however they are the least well understood of all the components. During the extended life test (ELT) conducted at JPL of the Deep Space 1 (DS1) flight spare NASA Solar Electric Propulsion Technology Applications Readiness (NSTAR) thruster, the longest life to date was demonstrated for a hollow cathode for electric propulsion. The test was voluntarily shut down after 30,352 hours[1] while the cathode assembly was still operational. However, the face of the keeper electrode has completely eroded away exposing the face plate of the hollow cathode. Post-test analysis of the cathode assembly suggested that one of the most likely near-term failure mechanisms for the engine would have been cathode failure due to the direct exposure of the discharge plasma to cathode orifice face plate.[2] In order to understand and predict keeper and subsequently the cathode failure mechanism a detailed modeling and experimental effort has been undertaken at JPL. The goal of the modeling effort has been to construct a self-consistent 2D model that can accurately predict the evolution of the plasma in all regions of the cathode.[3] The

---

[*] APT Staff, Advanced Propulsion Technology Group, Member AIAA
[†] Principal Scientist, Advanced Propulsion Technology Group, Senior Member AIAA
[‡] Member of the Technical Staff, Advanced Propulsion Technology Group, Member AIAA
[§] Member of the Engineering Staff, Advanced Propulsion Technology Group

model would subsequently be used to predict life and performance for several different cathodes which NASA utilizes. While the goal of the experimental effort, has been primarily to benchmark these physics models. The experiments have also been used to obtain data that will eventually be necessary to benchmark the models as they become more mature and sophisticated as more advanced physics are included.

The hollow cathode modeling effort at JPL has been a two step process. The first generation model, named IROrCa2D[3,4,5] is a 2D axisymmetric, time-independent code which models the insert/emitter region of the hollow cathode. This code is dependent on at least one plasma property measurement at the orifice entrance boundary.[4,5] This model has been benchmarked for two different cathodes, 1.5 cm diameter NEXIS and 0.635 cm diameter NSTAR cathode, with experimental axial data internal to the cathodes.[6,7,8] Plasma potential, plasma density, and electron temperature have all been obtained using high-speed axial internal Langmuir probes. The second generation model, named OrCa2D[4,5], is a 2D-axisymmetric, time-dependent code that models the plasma and neutral gas dynamics in the emitter, orifice, keeper, and plume regions. This second generation model is more advanced in its' physics and numerical approach. OrCa2D is self-reliant and does not depend on plasma property measurements as an input. Experimental data has been obtained internal to the cathode and external to the keeper in the anode region for both the NEXIS and NSTAR cathodes.[6,7,8] OrCa2D utilizes a flat plate anode to reduce complexity and to reduce computational time. The pervious experimental anode plasma measurements have been obtained also using high-speed axial Langmuir probes. However, the anode geometry plays an important role to the plasma potential structure, so in order to obtain a one-to-one comparison to OrCa2D simulations a circular flat plate anode has been installed 8.5 cm downstream of the keeper exit in the experimental setup. A radial Langmuir probe has also been utilized to obtain plasma measurements radially up to 1.8 cm downstream of the keeper, which further aids in a more complete data set for validation of the second generation model.

A unique feature to the OrCa2D model, is the inclusion of neutral gas dynamics. The model self-consistently solves the neutral gas momentum equation with viscosity, which yields neutral gas flux. In order to benchmark this neutral gas model, an optical technique is utilized to unfold local neutral density measurements in the near downstream plume region of the cathode. Based on the work of Yun and Tynan,[9,10] a fiber optic probe was used to measure photon production at a specific XeI downward transition.[11] The photon production rate is then directly proportional to neutral density.

For this experiment, plasma measurements are obtained for the NEXIS cathode with a circular flat plate placed 8.5 cm downstream of the keeper exit. Plasma potential, plasma density, and electron temperature measurements are presented axially and radially for cases (1) without an applied magnetic field, (2) 28 Gauss, (3) 56 Gauss, and (4) 78 Gauss of applied magnetic field. Local neutral density measurements are also presented for all fours cases.

II.   Experimental Hardware

A schematic illustration of the hollow cathode, anode, axial Langmuir cathode and anode probe assemblies, and radial scanning Langmuir and optical probes are shown in Figure 1. The cathode in these experiments has a conventional configuration of a barium impregnated tungsten insert in a 1.5 cm diameter molybdenum tube with a thoriated tungsten orifice plate e-beam welded on the end. A porous tungsten emitter impregnated with a low-work-function barium-calcium-aluminate mixture is located inside the cathode.[12] Electrons are emitted from this component by field-enhanced thermionic emission and travel through the orifice plate before entering the main discharge. The cathode is heated by a standard sheathed heater, which is turned off during discharge operation. A graphite keeper electrode fully encloses the cathode, and the keeper orifice is on the order of 2-3 mm.[6] The cathode and scanning probe system are mounted on an 8" Conflat flange installed in one port of 0.75-m diameter, 2-m long vacuum chamber. The chamber is pumped by two 10" CTI cryopumps with a combined xenon pumping speed of 1275 l/sec for xenon. The base pressure of the chamber is in the 1×10^{-8} Torr range, and during normal operation at less than 6 sccm of xenon flow the chamber pressure remains in the mid 10^{-5} Torr range, where the xenon gas is controlled and measured by a digital MKS mass flow controller. Additionally, a precision Baratron capacitive manometer is used to measure the pressure in the hollow cathode during operation.

The cathode is mounted in the vacuum system using the existing cathode scanning probe assembly[6] which shown in Figure 2a. The experimental arrangement uses a water-cooled circular flat plate anode that is approximately 15 cm in diameter, placed 8.5 cm downstream of the keeper exit. 8.5 cm was a constraint given by the physics model to which appropriate measurements and simulations could be compared. Also shown in Fig. 2a is a solenoid coil wound on a water cooled cylinder directly around the cathode to provide a diverging axial magnetic field of adjustable amplitude at the cathode exit that simulates the first ring of the cathode field in ring-cusp thrusters. See reference 6 for a full description of the cathode probe assembly.
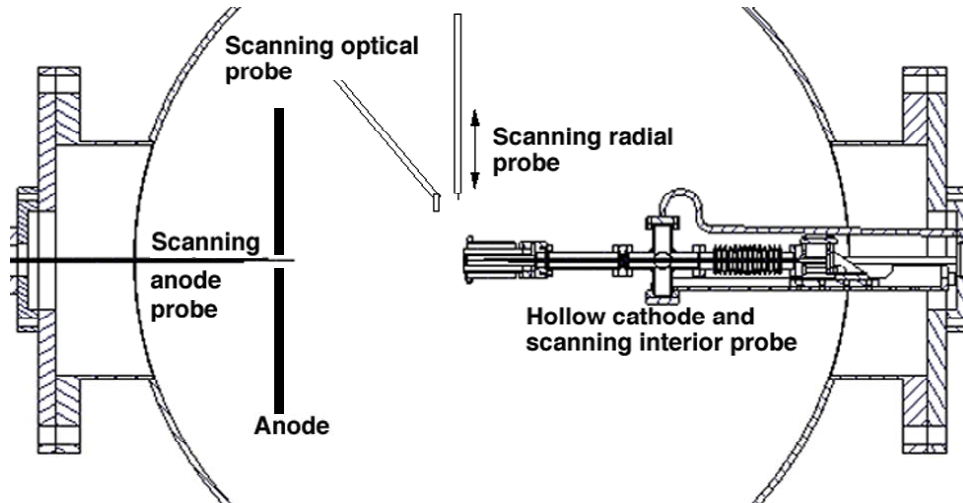
Figure 1. Schematic drawing of the cathode and anode placement along with the pneumatic scanning axial and radial probes relative to vacuum chamber.

The axial anode scanning-probe assembly is shown in Figure 2b, where the pneumatic plunger and vacuum bellows arrangement mounted on the outside of the vacuum system are seen. The diameter of the ceramic tubing interior to the vacuum system is stepped down from 3 mm to 0.5 mm diameter for the 2 cm section that is inserted deepest into the plasma in order to minimize perturbation to the plasma in the anode region. The exposed electrode is a 0.254 mm tungsten wire at a length of 1.15 mm to collect sufficient current away from the keeper region to accurately determine the plasma parameters. The anode probe has nearly 12 cm of unsupported length and a throw of almost 8 cm, so axial alignment is of concern. To minimize the axial misalignment, a 3 mm diameter hole was drilled in the center of the anode to support and guide the axial Langmuir probe. The hole is large enough for the 3mm ceramic tube to clear the guide, while being kept as minimal as possible as to not disturb or change the conduction of the plasma to the anode. The larger 3 mm ceramic tube protrudes out of the anode .2 cm to ensure that when the anode probe is in the full back position, it does not slip out of the centered guide and cause damage to the probe, this can also be seen if Figure 2a. The axial probe moves at one meter a second with a position resolution of 0.5 mm. Very careful iterative alignment techniques are used to ensure that the anode probe is aligned with the
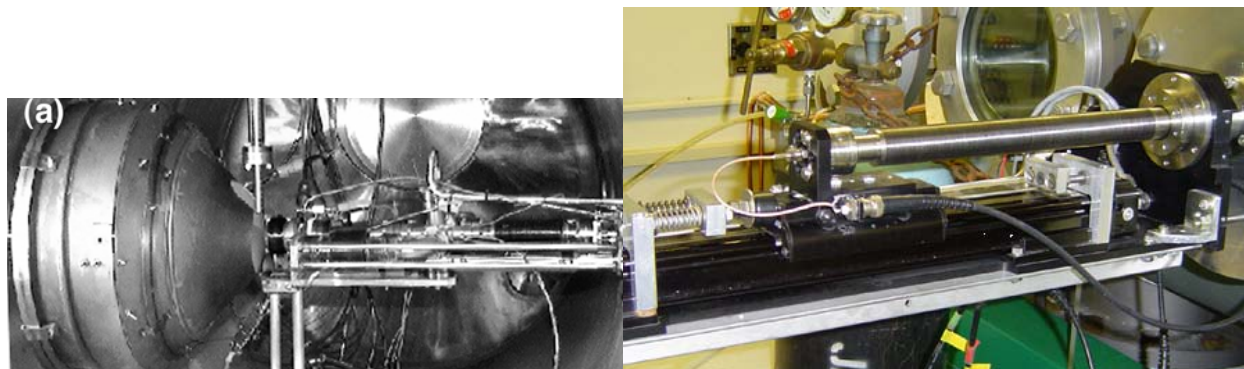

Figure 2. Scanning probe assemblies (a) cathode mounted in the vacuum chamber with the cylindrical flat plate water cooled anode with solenoidal magnetic coil around the cathode, and (b) the anode probe drive system outside the vacuum system showing the high speed pneumatic plunger and bellows arrangement.

cathode orifice and within 0.5 mm of the centerline. The anode probe can be fully inserted into the keeper orifice, although whip of the long ceramic sometimes causes the tip to touch the keeper or cathode during retraction.

A radially scanning Langmuir probe can be seen in Figure 1 and 2b. It uses a pneumatic plunger, identical to the cathode plunger, and is mounted to a Huntington X-Y manipulator outside the vacuum system to provide positioning relative to the keeper exit point. . The radial probe has a linear throw of 3 cm, also at one meter per

second, and is aligned by a slide-guide internal to the vacuum system to obtain a position resolution of 0.25 mm. The probe can be positioned in front of the keeper as close as 2 mm out to 1.8 cm downstream. The probe tip is a 0.127 mm diameter tungsten wire feed through a 0.5 mm diameter alumina tube protruding 1.0 mm. When the Langmuir probe is not in use, it resides in 6.5 mm tube which is sufficiently out of the discharge plume to protect it from ion bombardment.

In order to take Langmuir traces through both probes, a bias voltage applied to the probe tips is generated by a programmable waveform synthesizer that drives a Kepco bipolar power supply. The voltage waveform is a sawtooth ramp that scans from –10 to + 50 V in the anode region, in a time of 2.5 msec for the anode probe and 1.5 msec for the radial probe. A delay generator is used to take consecutive traces allowing the cathode plasma parameters can be mapped. Electron temperatures and plasma potentials are determined in less than half of a total trace therefore the position uncertainty for the plasma parameters is on the order of 0.5 mm over most of the scan and less than 0.25 mm near the full insertion point. The probe position, voltage and current data is collected on a PC at a sample rate of 275 kHz, resulting in 275 data points in each probe characteristic curve. The plasma potential and electron temperatures are found by classical Langmuir probe analysis. The electron temperature is found by fitting an exponential curve to the electron retardation region of the Langmuir trace.. The electron temperatures have error bars about ±0.5 V and the plasma potentials have error bars of up to ± 2V in the anode region.

The optical probe is made of a blank diameter optical fiber. This fiber is appropriate for this wavelength range, which the 823.1nm line falls under. The probe consists of a 0.25" stainless steel tube stepped down to a 0.125"
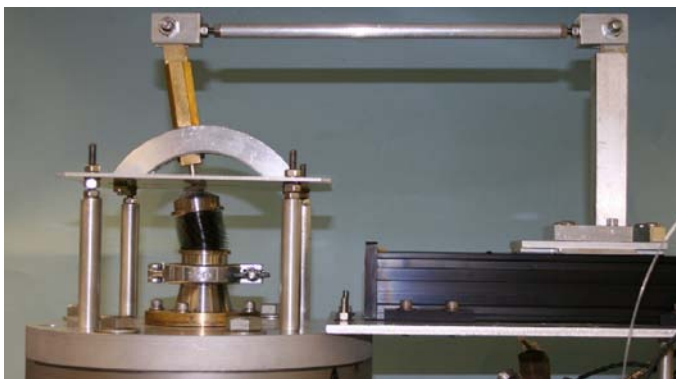

Figure 3. (a) The radial optical probe assembly system outside the vacuum system showing the linear probe drive along with the bellows arrangement.

stainless steel tube to fit snugly around the fiber. Assume fiber is taken as a point source, the fiber is recessed in the tube 1.5" to obtain a resolution of 1-1.5mm. The 0.25" tube is connected to the bellows arrangement which can be seen in Figure 3. The probe is driven by a linear probe drive which is driven by a crappy stepper motor. The stepper motor is controlled by a certain program on the computer. The probe is swept on a time scale of this to collect sufficient line intensity at each spatial resolution. Even though the sweep is a an ark, the length of the tube is long enough and the radial distance of interest is small enough that the radial sweep measurements are not on an ark.

III.   Experimental Results

For validation of the present simulations of the OrCa2D code, plasma properties are found using the previously mentioned array of probes. At the present time the simulations of the code are conducted without a magnetic field, however future plans are to impose an applied magnetic field. Experimental results are found for (1) a case without an applied magnetic field, (2) 28 Gauss of applied field, (3) 56 Gauss of applied magnetic field, and (4) 78 Gauss of applied field. The 78 Gauss case is the nominal field strength around the cathode for the NEXIS engine. Figure 4 shows photographs of the discharge running in all four cases. For the first case, without and applied field, the discharge current is slightly higher then the nominal 25 Amperes. To obtain a stable discharge, at least 27.5A of discharge current was necessary to keep the plasma from entering into discharge power supply oscillations. For cases with applied magnetic field, the plasma has enough energy to carry the current to the anode and 25A of discharge current was sufficient to sustain a stable discharge.
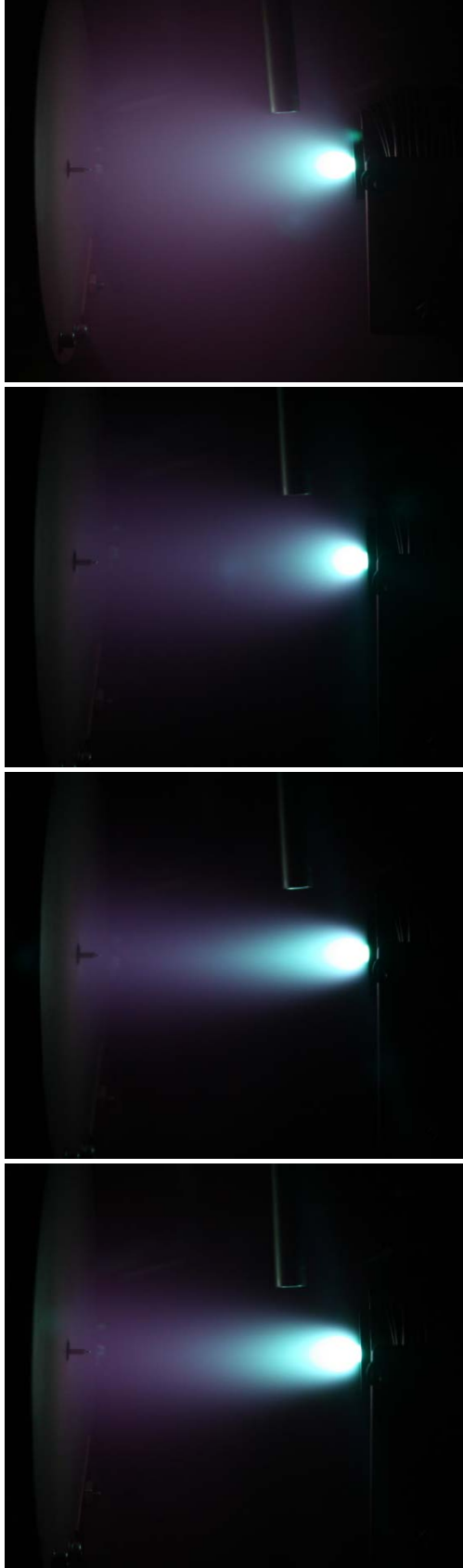
Figure 4. Discharge Plasma for 0G (a), 28G (b), 56 G (c), and 78G (d).

The first thing to notice is that without an applied magnetic field, the electrons are not as confined and the plume is much more divergent than the cases with an applied field. As the magnetic field strength is increased the plasma becomes more collimated and the structure of the bright spot or "plasma ball" just downstream of the keeper changes. This set of pictures was taken at 1/50 of a second. To visually investigate the structure of the ball in each case, pictures were taken at a much faster shutter speed, at 1/2500 of a second. Figure 5 shows the plasma ball for each case. In Figure 5, there is the previously described[6,7,8] dark space for each ball structure. However, the plasma protruding from the keeper orifice upstream of the dark space has a different structure and also appears to be radiating at a different at a different optical line than the bulk plasma ball for each case.

The plasma ball is a complex in nature and difficult to probe due to its proximity to the keeper. This investigation focuses on the ball when finding both plasma parameters and photon production rate.

A. Plasma Density Measurements

The plasma density in the keeper region is found from taking position scans with the probe biased to ion saturation current. In this region, the plasma density should be sufficiently high that the sheath is small compared to the probe radius and the probe data can be analyzed in the "thin-sheath" regime. The plasma density in the thin sheath regime is evaluated from the current[13,14] given by:

$$I = \beta \, n \, e \sqrt{\frac{kT_e}{M}} \, A \qquad (1)$$

where β is a coefficient that changes with the geometry and the collisionality of the plasma, n is the density, e is electron charge, kT_e is the electron temperature, M is the ion mass, and A is the area of the probe If the plasma is in a collisionless regime, β is conventionally given as 0.5 from the Bohm current[13,14] The appropriateness of the probe theory used (thin or thick sheath) was checked by calculating the ratio of the Debye length to the probe radius. The probe radius was sized for the entire throw of the axial anode probe to be in thin sheath regime.

The electron temperature used for evaluating the density is obtained from the Langmuir probe analysis as described above. The NEXIS engine has six magnetic rings, with the cathode ring at a field strength of 78 Gauss. In these experiments, the case where there no applied magnetic field is strictly for the purposes of code validation and gain understanding of the physics of cathode plumes. The case where 78 Gauss is applied would be more representative of the cathode plume in the engine. The axial plasma density profiles measured by the anode probe for 0G and 78G are shown in Figure 6a. The plasma density for the case of 78G is 15-35% higher than the case with any magnetic field out to

5

Figure 5. Plasma ball in the cathode plume for 0G (a), 28G (b), 56G (c), and 78G (d).

4.5 cm downstream of the cathode. The largest difference in density occurs is in the first 0.5 cm of the keeper exit, where the plasma ball is present. This affect can better be seen in Figure 6b where the 0.5 cm downstream of the keeper is plotted on a linear scale. Figure 5a shows that the plasma ball is closest the keeper orifice, without a magnetic field where the density profile drops drastically downstream of the keeper exit. Figure 5d shows that the orifice plasma is extended 3-4 mm downstream before the familiar plasma ball is present. The plasma density profile for 78 Gauss has a flatter slope in the orifice and then continues to fall drastically. Both profiles show an order of magnitude drop by the first downstream centimeter and two orders of magnitude by 4.5 centimeters downstream. For the 78 Gauss case, there are diverging axial field lines which the electrons follow, and the density will decrease on axis for this case.

The radial Langmuir probe has been used to obtain plasma density contours downstream of the keeper from 0.3 cm-1.8 cm. The farthest downstream position is constrained by the radial probe geometry in the vacuum chamber. However, 1.8 cm downstream of the keeper is sufficient to be out of the plasma ball, which can be seen in Figure 4 where the radial probe housing tube is at this last axial position. Figure 7 shows contours for both cases without and with 78 Gauss. The two contours verify that the plasma density in the plasma ball region is about 20% higher for the case with magnetic field. Also the contour with magnetic field shows that the plasma is collimated in the plume region which can visually be seen in Figure 4d compared to Figure 4a.
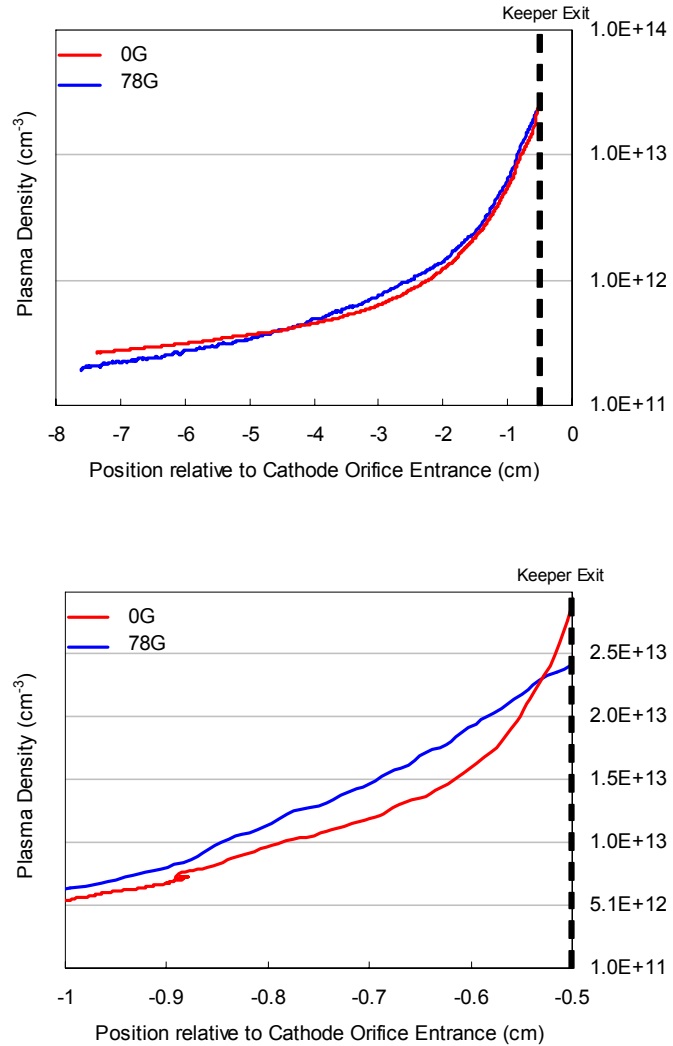

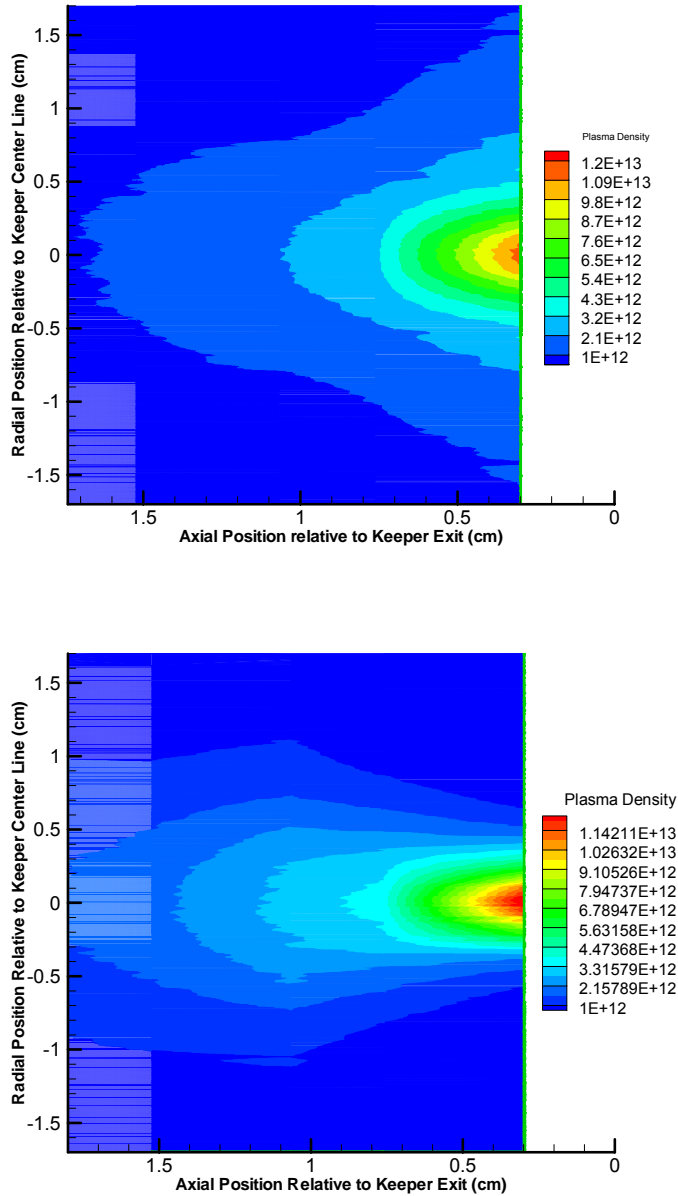**Figure 6. Axial anode density profiles plotted on (a) a semi-log scale, (b) on a linear scale for 0G and 78G.**

B. Plasma Potential and Electron Temperature Measurements

The axial plasma potential and temperature profiles for the anode are shown in Figure 8. The plasma potential for 0 G case increases as you move downstream of the keeper. This trend has been consistent with previous axial anode measurements for various different anode geometries.[6,7,8] The potential inside of the cathode has been found to be insensitive to the anode geometry and a plasma potential inside keeper orifice of approximately 12 V which is also consistent with pervious measurements. The axial plasma potential for the 78 G case has a slightly different profile. Moving downstream the potential increases until about 3.5 cm and there is a 2 V drop and then the plasma potential again begins to increase. Comparing this potential change at the specific axial position to the photograph in Figure 4d, shows an approximate agreement because of the transition from the ball-plume to the pinker bulk plasma in the vicinity potential change. Another curious point is that the axial plasma potential for both cases never reach the discharge voltage. The discharge voltage for the 0G case is 24.4V and for 78G is 19.1V. The 2D contours of the plasma potential for both cases can be seen in Figure 9. The plasma potential in the radial direction is a minimum on the centerline, causing a potential well. However, for the case of 78 G the potential difference is larger due to the large discharge voltage. From pervious steady state emissive probe measurements[7], the peak radial potential is slightly higher then discharge voltage which is constant to the contours closest to the keeper exit. In the 78G case, the electrons are confined to the magnetic field lines also allowing the plasma potential to be larger compared to the case without a magnetic field.
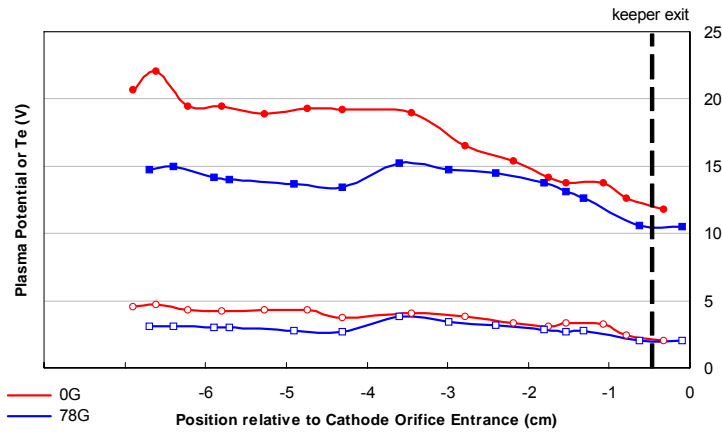

Figure 7. Plasma density contours for the keeper region for (a) 0G and (b) 78G.

The axial electron temperature for both cases can also be seen in Figure 8. The electron temperature for both cases seems to be correlated to the plasma potential. As the plasma potential increases the electrons are accelerated causing the electron temperature to increase. The 2D contours for the electron temperature are shown in Figure 10. The electrons have to have more energy to cross field lines causing the electron temperature to increase. However the radial profiles don't follow the same rational. At the closest axial position to the keeper where the field lines would be the strongest, the 78G case, the radial plasma potential increases while the electron temperature starts to decease once a peak is reached. The peak electron temperature does increase as it moves downstream and the temperature well becomes wider. For the 0G case, there is also a temperature well and the peak temperature at the edge of the well also increases as it moves downstream.

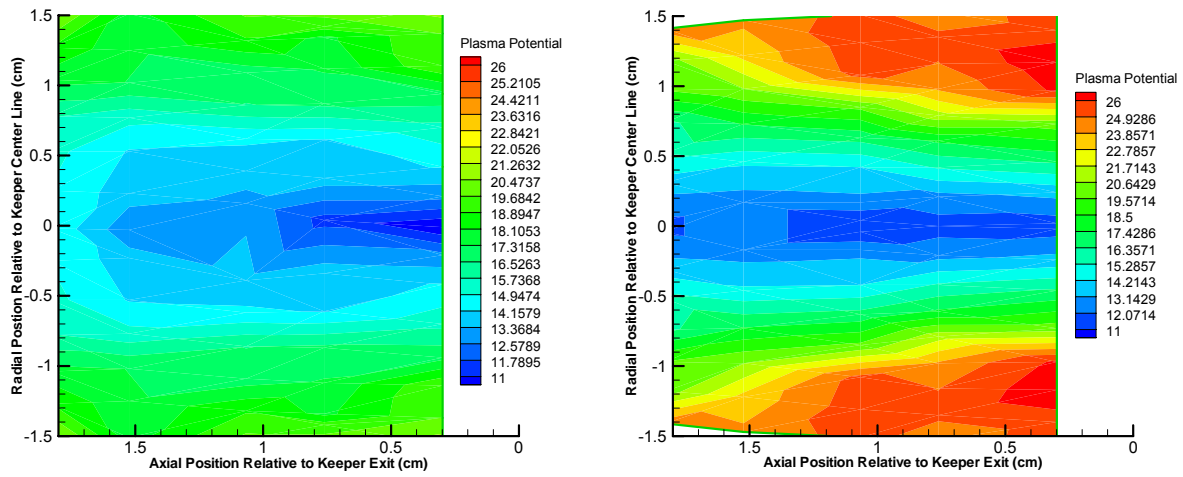**Figure 8. Axial anode plasma potential and electron temperature profiles for 0G and 78G.**

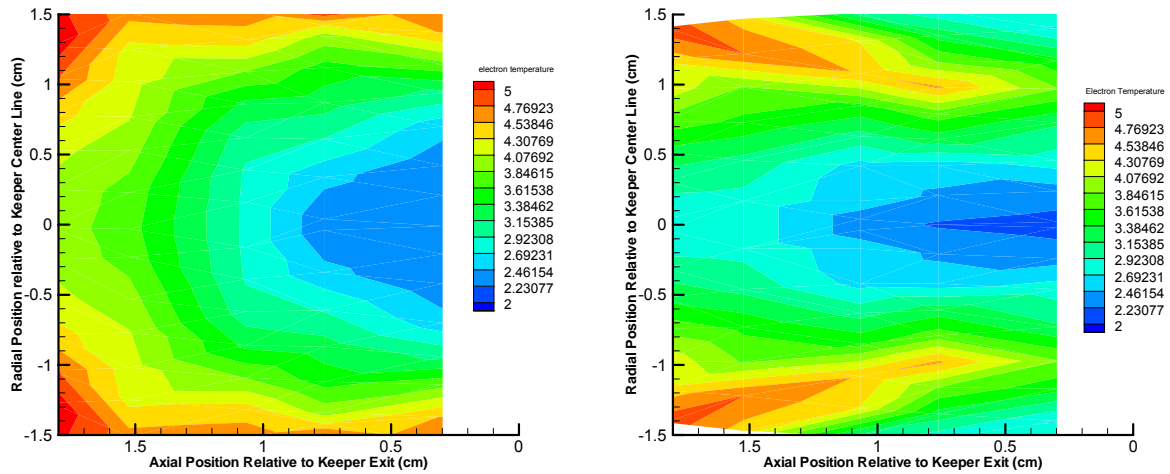**Figure 9. Plasma potential contours for (a) 0G and (b) 78G.**

Figure 10. Electron temperature contours for (a) 0G and (b) 78G.

8

C. Optical Probe Measurements

Optical emission spectroscopy was used to measure local xenon neutral density in the cathode plume region. The rate at which excited XeI atoms emit a photon from a downward transition from state j to i is related to the XeI production rate as follows,

$$J_{ji} = n_o n \sigma_* v V \qquad (2)$$

where Jji is the production rate in photons per second, n_o is the neutral density, n is the density, σ_* is the excitation cross section, v is the velocity of the particle, and V is volume over the measured excitation collection. The density will be taken as the density distribution over the electron velocity $n=n_e(v_e)$. $\sigma_* v$ is the excitation reaction rate over the electron velocity, so $\sigma_* v = \sigma_* v_e$. The production rate then becomes,

$$J_{ji} = n_o n_e(v_e) \sigma_* v_e V$$

$$J_{ji} = \int_{v_{th}}^{\infty} n_o n_e f(v_e) \sigma_* v V dv_e$$

where n_e is now the total electron number density and $f(v_e)$ is the electron velocity distribution function. If n_o is constant then it can be pulled out of the integral, integrate over a maxwellian electron velocity distribution function, and then the production rate becomes,

$$J_{ji} = n_o n_e V \int_{v_{th}}^{\infty} f(v_e) \sigma_* v dv_e = n_o n_e \langle \sigma_* v_e \rangle V$$

where $< \sigma_* v_e >$ is called the excitation reaction rate. The excitation cross section σ_* in m^2 can be found in the literature. For the excitation reaction rate calculations used in this experiment, excitation cross section data will be taken as the Hayashi cross section data.[14]

To measure the photon production rate for excited neutrals, the intensity of a specific spectral line was measured. One of the strongest neutral lines is at 823.1nm, this is $6p[3/2]_2$ -$6s[3/2]^0_2$ transition and when measured it gave the strongest signal to noise ratio. The optical probe is a collimated fiber and as it scans radially across the plume, it is averaging the light intensity over a cord at each radial location. In order to unfold a profile of line intensity radially, the cord averaged data was Abel inverted. The line averaged measurement is related to radial profile by,
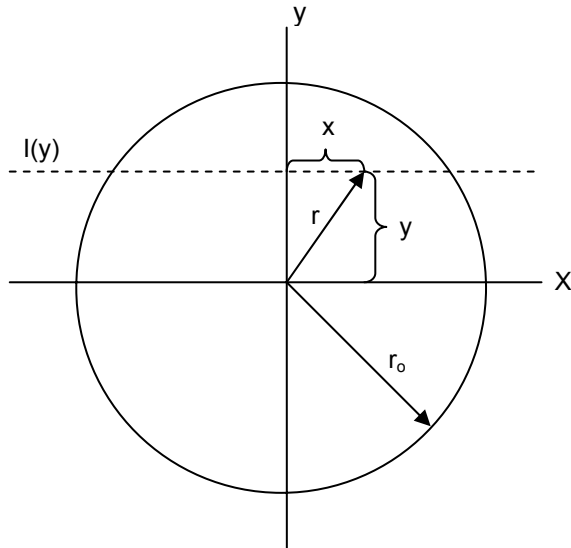

Figure 11. Drawing of relationship between a cord measurement and a radial measurement.

$$I(y) = 2\int_0^{(r_o^2 - y^2)^{1/2}} \varepsilon(r) dy$$

where I(y) is the measured cord averaged line intensity, $\varepsilon(r)$ is the radial profile of the line intensity, r_o is the radius of the cylinder, and y is at a given radial location. These variables are visually represented in Figure 11. Equation 6 can be converted in to radial coordinates, given as,

$$I(y) = 2\int_y^{r_o} \frac{\varepsilon(r) r dr}{(r^2 - y^2)^{1/2}}$$

Lastly the equation 7 can be inverted using Abel inversion to give the radial profile as,

$$\varepsilon(r) = \frac{-1}{\pi} \int_y^{r_o} \frac{I'(y)}{(y^2 - r^2)^{\frac{1}{2}}} dy$$

where I'(y) is the derivative of the cord averaged line intensity probe signal. The cord averaged signal was Abel inverted and the contour plots are shown in Figure 12.

The measured intensity is the strongest on axis for both cases without and with 78 G. The contour in Figure 12b
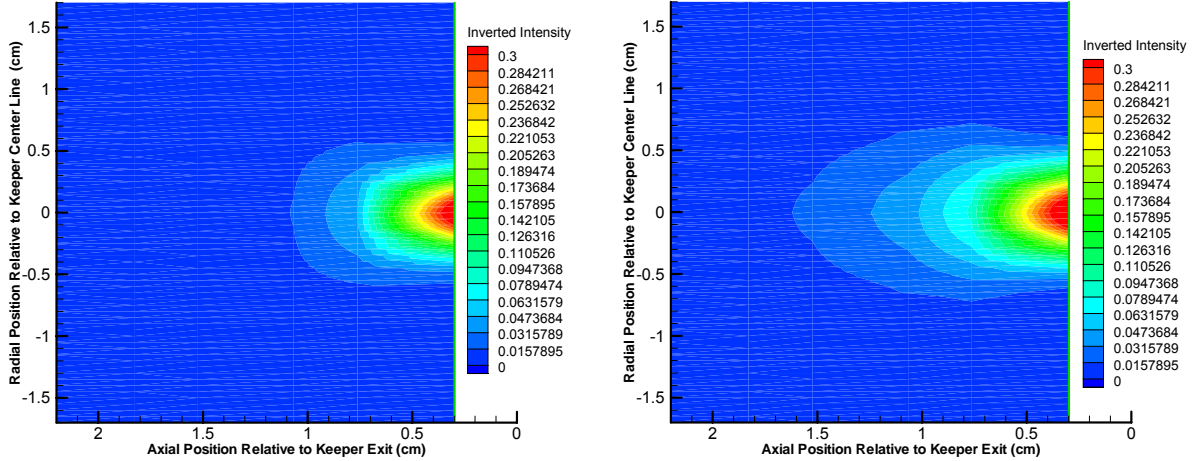

Figure 12. Radial contour profiles on 823.1 nm line intensity for (a) 0G and (b) 78G.

shows that the strongest signal is extended farther down stream than in the case with out magnetic field, shown in Figure 12a. Also weaker light intensity is detected farther downstream. It looks like the plume is larger in the case with magnetic field, but these contours show the excited neutrals. If the electrons are confined as they are in the case with magnetic field then the it is more likely that an electron will make an inelastic collision and excite a neutral. This is consistent with Figure 4b when ball is extended and brighter.

D. Neutral Density Profiles

The local neutral density can be deduced from equation 5, given as,

$$n_o = \frac{J_{ji}}{n_e \langle \sigma_* v_e \rangle V}$$

The production rate in relative terms is given in section C, plasma density and electron temperature for the same spatial location as the measured relative production rate were given in sections A and B, respectively. The volume of the measured excited region is known from the geometry of the probe. It is taken to be a cylinder with the diameter of the exposed optical fiber and the length being the integrated collection area of the probe.

Local neutral density profiles are shown in Figure 12. The first thing to notice is that the neutral profiles are not the same. Neutrals are not affected by magnetic field lines and should not fell there presence. Neutral pressure will change with the amount of ionization. However, the percentage ionization is very small, on the order of 10% or less and the difference between the two contour plots is much greater than 10%. The plume has two populations of electrons, the maxwellian distribution of electrons and primaries electrons. Both of which will contribute to the excitation of neutrals, and the intensity measured by the optical probe. The photon production rate is then the sum of the production rate by the maxwellian distribution and the production rate of the primaries given by,

$$J_{ji} = J_{ji\,\mathbf{max}\,wellian} + J_{jiprimaries}$$

10
American Institute of Aeronautics and Astronautics

The number of primaries should be the same for both cases but there are confined with the 78G and will have a greater affect to the production rate of photons, which again is present visually in Figure 4d compared to Figure 4a. the total production rate for neutral excitation is given by,

$$J_{ji} = J_{ji_{max}} + J_{ji_{prim}} = n_o n_e \left\langle \sigma_* v_{e_{max}} \right\rangle V + n_o n_e \left\langle \sigma_* v_{e_{prim}} \right\rangle V$$

In the calculation of the local neutral density, only the production from the maxwellian distribution is considered and this causes the neutral density to appear larger.
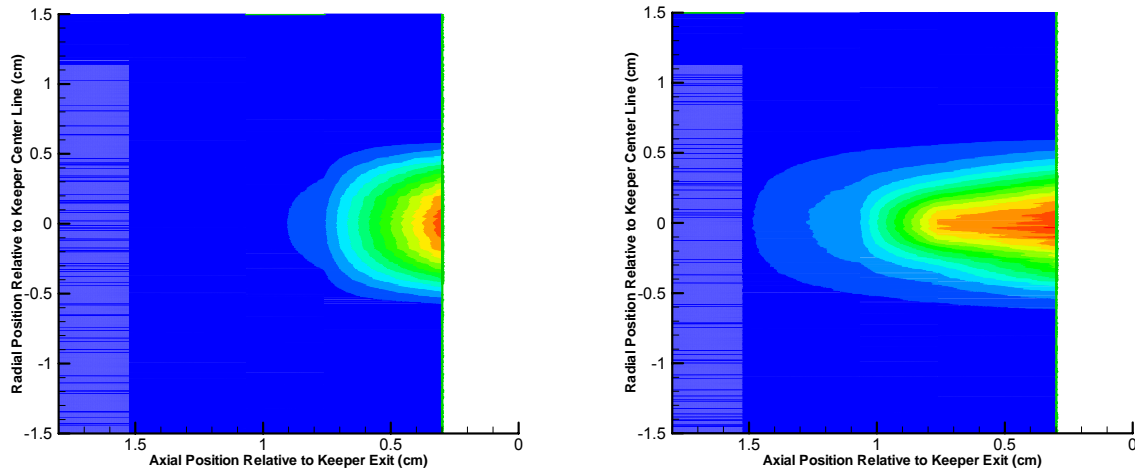

Figure 13. Local neutral density contour profiles for (a) 0G and (b) 78G.

IV.   Discussion

Due to the constrains given by the model the anode had to be places 8.5 cm downstream of the keeper. The OrCa2D model is running simulations without an applied axial magnetic field. The nominal case for the NEXIS cathode is run with 25A of discharge current, however without any magnetic field, the plasma was unstable at 25A. The plasma at this operating condition and geometry, can not conduct the current anode. The primaries are not confined and are lost leading to the observed instabilities and subsequent raising of the discharge current until the plasma became stable. In future generations of the model, the anode geometry will not be as strictly confined so close to the keeper. If the plate was placed further downstream, the plasma would have an easier time conducting to the anode allowing for a stable plasma at 25A of discharge current.

Many of the measurements presented in the paper are assuming a maxwellian energy distribution function for the electrons (EEDF), which could be problematic for many of the measurements if it is not strictly a maxwellian. The neutral excitation reaction rates for example integrates the excitation cross section over a maxwellian distribution, where we know that the primaries will have an effect on the neutral plasma density, shown in Figure 13. If the distribution function has a high energy tail, which the primaries would add to the EEFD, then the reaction rates could change significantly. If the EEDF was known, this would also affect the interpretation of the electron temperature. It was seen that electron temperature increases radially from the centerline. The interpretation is that the electrons now have a maxwellian distribution centered at 3 eV. However if the EEDF is a drifted maxwellian then the electron temperature would also be perceived as higher. If the EEDF was known then a better understanding of the data could be obtained. Another difficulty is in measuring the plasma parameters in the plasma ball with a Langmuir probe. Downstream, closer to the anode the Langmuir trace has a clear break and the plasma parameters and be determined with confidence. As the Langmuir probe is scanned closer to the keeper in the plasma ball, the Langmuir trace becomes harder to interpret duo rounding of the trace. This rounding is most likely due to

the presence of primary electrons. If the EEDF was know then the Langmuir trace could more accurately analyzed to obtain the appropriate plasma parameters.

Lastly, the pictures of the plume with a fast shutter speed show that there is a color change between the green plasma in the keeper orifice and the blue plasma after the dark space.   It has been suggested that the difference between the blue and green plasma is the difference in ionization potentials. However the difference between the two visual lines 0.03 V and is not likely to be the cause color change. It has also been suggested that the green is indicative of a strongly ionized plasma, while the blue is a combination of green ions and pink neutrals.

V.   Conclusion

These profiles are the first step in understanding the plasma proprieties in the cathode plume. Accurate measurements will not only aid in validating the OrCa2D code, they will also become inputs for for discharge models like DC-ION and HP-Hall. But for these measurements to be as accurate as possible and to be understood, the electron energy distribution must be known in the plume region. The next natural step is to experimentally determine the EEDF.

Acknowledgments

References

[1]A. Sengupta, J. Brophy, K. Goodfellow, "Status of the Extended Lift Test of the Deep Space 1 Flight Spare Ion Engine After 30'352 Hours of Operation", AIAA Paper #2003-4558, 39th Joint Propulsion Conference, Huntsville, AL, July 20-23, 2003.

[2]A.Senupta, et al., NASA T/TP 2004-213391, (2004).

[3]I. Mikellides, I. Katz, D. Goebel, J. Polk, "Theoretical Model of a Hollow Cathode Insert Plasma", AIAA Paper #2004-3817, 40th Joint Propulsion Conference, Ft. Lauderdale, FL, July 11-14, 2004.

[4]I. Mikellides, I. Katz, D. Goebel, J. Polk, "Theoretical Model of a Hollow Cathode Plasma for the Assesment of Insert and Keeper Lifetimes", AIAA Paper #2005-4234, 41st Joint Propulsion Conference, Tucson, AZ, July 10-13, 2005.

[5]I. Mikellides, I. Katz, D. Goebel, "Numerical Simulation of the Hollow Cathode Discharge Plasma Dynamics", IEPC Paper ___, 29th International Electric Propulsion Conference, Princeton, NJ, October 31-November 4, 2005.

[6]D.M.Goebel, K.Jameson, R.Watkins, I.Katz, "Hollow Cathode and Keeper-Region Plasma Measurements Using Ultra-Fast Miniature Scanning Probes', AIAA Paper #2004-3430, 40th Joint Propulsion Conference, Ft. Lauderdale, FL, July 11-14, 2004.

[7]K.Jameson, D.M.Goebel, R.Watkins, "Hollow Cathode and Keeper-Region Plasma Measurements", AIAA Paper #2005-3430, 41st Joint Propulsion Conference, Tucson, AZ, July 10-13, 2005.

[8]K.Jameson, D.M.Goebel, R.Watkins, "Hollow Cathode and Thruster Discharge Chamber Plasma Measurements Using High-Speed Scanning Probes", IEPC Paper IEPC-2005-269, 29th International Electric Propulsion Conference, Princeton, NJ, October 31-November 4, 2005.

[9]S. Yun, et.al., "Neutral Uniformity and Transport mechanisms for Plasma Etching", Physics of Plasma, (8) 6, June 2001.

[10]S. Yun, et. al., "Measurements of Radial Neutral Pressure and Plasma Density Profiles in Various Plasma Conditions in Large-Area High-Density Plasma Sources", Physics of Plasma, (7) 8, August 2000.

[11]A.Sengupta, D.M. Goebel, D. Fitzgerald, A. Owens, "Experimentally Determined Neutral Density and Plasma Parameters in a30 cm Ion Engine", AIAA Paper #2004-3613, 40th Joint Propulsion Conference, Ft. Lauderdale, FL, July 11-14, 2004.

[12]J. Brophy, "NASA's Deep Space 1 Ion Engine", Rev. Sci.Instrum. **73** (2002) p.1071-1078

[13]F.Chen, ""Electric Probes", in *Plasma Diagnostics Techniques* (ed. R. Huddelstone and S. Leonard), Academic Press, NY (1966) p. 113-200.

[14]D.Bohm, *The Characteristics of Electrical Discharges in Magnetic Fields*, edited by A. Gutirie and R.K. Wakerling (McGraw-Hill, New York, 1949) Chap.3.